A. M. Waas[1]
Graduate Research Assistant,
Mem. ASME

C. D. Babcock, Jr.[2]
Professor of Aeronautics and
Applied Mechanics,
Mem. ASME

W. G. Knauss
Professor of Aeronautics and
Applied Mechanics,
Mem. ASME

Graduate Aeronautical Laboratories,
California Institute of Technology,
Pasadena, CA 91125

A Mechanical Model for Elastic Fiber Microbuckling

A two-dimensional mechanical model is presented to predict the compressive strength of unidirectional fiber composites using technical beam theory and classical elasticity. First, a single fiber resting on a matrix half-plane is considered. Next, a more elaborate analysis of a uniformly laminated, unidirectional fiber composite half-plane is presented. The model configuration incorporates a free edge which introduces a buckling mode that originates at the free edge and decays into the interior of the half-plane. It is demonstrated that for composites of low volume fraction (<0.3), this decay mode furnishes values of buckling strain that are below the values predicted by the Rosen (1965) model. At a higher volume fraction the buckling mode corresponds to a half wavelength that is in violation of the usual assumptions of beam theory. Causes for deviations of the model prediction from existing experimental results are discussed.

1 Introduction

A problem that has received much attention but moderate success is the prediction of compressive strength of fiber composites. Dow and Gruntfest (1960) were apparently the first to identify fiber buckling as a viable mode of compressive failure in composites. Their work was followed by that of Fried and Kaminetsky (1964) and Leventz (1964), who addressed experimentally and theoretically the question of compressive strength. In these investigations, an empirical factor was used to obtain a correlation between the experimentally and theoretically predicted values of compressive strength. In 1965, Rosen (1965) presented an analysis addressing the question of microbuckling which was devoid of any empiricism and laid the foundation for much of the work that was to follow. With a few exceptions, noted later, the analytical research work carried out in the past 20 years is based on the model by Rosen (1965). Due to lack of space and because an excellent literature survey on fiber microbuckling exists (Shuart (1985)), a discussion of the various contributions that have enhanced our understanding of microbuckling will be omitted here. Instead, the discussion will be limited to those aspects that are fundamental in clarifying the state-of-the-art of the subject. The interested reader is referred to the references at the end of this chapter and the review by Shuart (1985), in particular, for a complete and up-to-date account.

The Rosen (1965) model for microbuckling addresses the problem of fiber buckling in glass fiber/epoxy laminates under compressive loading. The model presented, which is two-dimensional, treats the fiber layers as plates supported by an elastic matrix (offering lateral support to the fibers at buckling). When the unidirectional composite of infinite extent undergoes failure, Rosen envisages two possible modes of failure which he calls the extension and shear modes. In the extension mode, the matrix material is predominantly in extension and adjacent fibers deform 180 deg out of phase with each other, as shown in Fig. 1. In the shear mode, adjacent fibers deform in phase, and the matrix material is

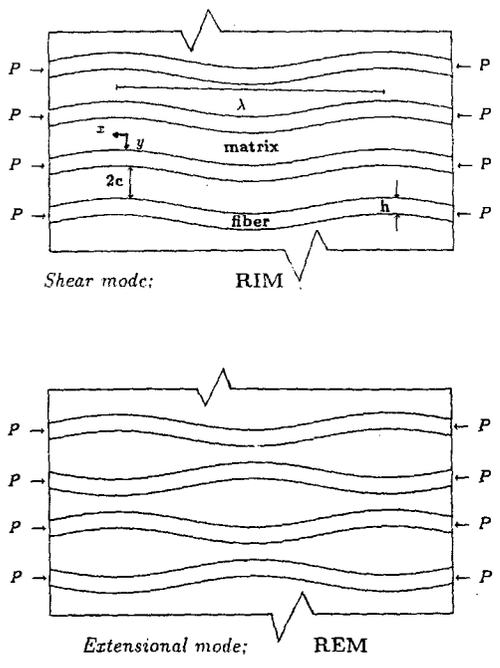

Fig. 1 The configuration studied by Rosen (1965)

[1]Presently at the Department of Aerospace Engineering, University of Michigan, Ann Arbor, MI 48109.

[2]Deceased.

Contributed by the Applied Mechanics Division of THE AMERICAN SOCIETY OF MECHANICAL ENGINEERS for publication in the JOURNAL OF APPLIED MECHANICS.

Discussion on this paper should be addressed to the Technical Editor, Leon M. Keer, The Technological Institute, Northwestern University, Evanston, IL 60208, and will be accepted until two months after final publication of the paper itself in the JOURNAL OF APPLIED MECHANICS. Manuscript received by the ASME Applied Mechanics Division, September 12, 1988; final revision, June 6, 1989.

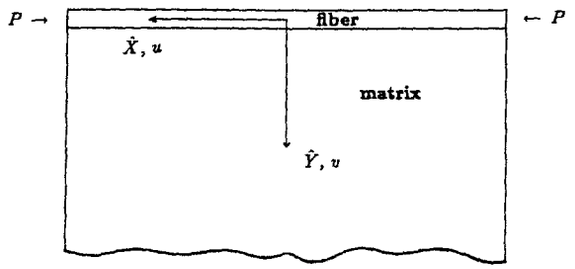

Fig. 2(a) The single fiber composite

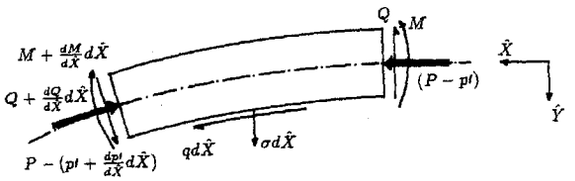

Fig. 2(b) Isolated element of buckled fiber

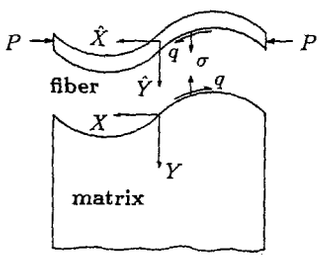

Fig. 2(c) Matrix configuration at buckling

predominantly in shear. Using an energy method to obtain the buckling load, Rosen approximated the buckled mode shape of the fibers to be

$$v = \sum_{n=1}^{\infty} a_n \sin\left(\frac{n\pi x}{L}\right).$$

Here, $L/m = \lambda$, the buckle wavelength, as indicated in Fig. 1. In evaluating the contribution to the potential energy from the matrix at buckling, he assumed the *strains* in the matrix to be independent of y. This amounts to approximating the displacements in the matrix to vary linearly in y. Next, considering the bending energy contribution of the fiber and the work done by the in-plane compressive loads on the fiber, he obtains the following critical values for the extensional and shear modes:

Extensional Mode:

$$\sigma_{cr} = 2V_f\left[\frac{V_f E_m E_f}{3(1-V_f)}\right]^{1/2} \tag{1}$$

$$\left(\frac{\lambda}{h}\right)_{cr} = \pi\sqrt[4]{\frac{(1-V_f)}{3V_f}\frac{E_f}{E_m}}. \tag{2}$$

Shear Mode:

$$\sigma_{cr} = \frac{G_m}{1-V_f} + O\left(\left(\frac{h}{\lambda}\right)^2\right) \tag{3}$$

$$\left(\frac{\lambda}{h}\right)_{cr} \gg 1. \tag{4}$$

Here, σ_{cr} = critical compressive stress at buckling, E_m = Young's modulus of the matrix, E_f = Young's modulus of the fiber, V_f = volume fraction of fibers, h = thickness of a fiber plate, and λ = wavelength of the buckled fiber.

Notice that in the shear mode the critical value of σ occurs for $\lambda \gg h$. Thus, unlike the extension mode in which a critical buckle wavelength can be evaluated, no such value λ_{cr} exists in the shear mode. The buckling "load" is continuously dependent on the wavelength λ.

A second viewpoint regarding the mode of failure in compression is referred to as *fiber kinking*. Observations on kinking failure go back as far as 1949 when Orowan (1942) observed that single crystal rods of Cadmium collapse under uniaxial compression into peculiar kinks if the (0001) glide plane is nearly parallel to the axis of compression. It is frequently useful to use four axes (thus four Miller indices), three of them co-planar, to describe the crystal planes for hexagonally close packed (HCP) crystals. The (0001) for HCP Cadmium is the basal plane. The advent of fibrous materials has rekindled interest in the subject, and in recent years, fiber kinking as a viable mode of failure has been observed by, among others, Weaver and Williams (1975), as well as other researchers (Dale and Baer, 1974; Robinson et al., 1986, Evans and Adler, 1983; Chaplin, 1977). Judging from the experimental evidence available, it appears that the formation of compression-induced kink bands is closely associated with the existence of a preferable glide plane in the direction of compression. Budiansky (1983) analyzed kinking by introducing inelastic behavior in the matrix and explained the large scatter in kinking strengths in terms of the composite's sensitivity to initial fiber misalignment. He presents in Budiansky (1983) a result for the compressive strength of the composite which depends on the matrix yield stress in shear and on the initial fiber misalignment. However, the experimental evidence available (Fried and Kaminetsky, 1964; Leventz, 1964; Hahn and Williams, 1986; Sohi, Hahn, and Williams, 1984; Hahn, Sohi, and Moon, 1986; Lager and June, 1969) does not suggest that kinking failures are limited to composites that permit inelastic matrix behavior.

More recently, Hahn and Williams (1986) and Sohi et al. (1984) have reported experimental results related to compression failure in straight fiber-laminated test specimens. In these studies, it was repeatedly observed that failure of the fibers in plies aligned along the loading direction (0 deg plies) originated at a *free edge* and subsequently propagated into the interior of the specimen, precipitating a global failure of the test specimen. This observation is consistent with the findings of Waas and Babcock (1989) as regards the origins of the failure process.

In this paper we consider a simple mechanical model that is capable of demonstrating the origins of compressive failure at a free edge. To do so, the problem of a laminated half-plane subjected to a uniform far-field compression parallel to the surface of the half-plane is considered. Despite the fact that experimental observations strongly suggest that fiber-microbuckling originates at a free edge, a model configuration that allows incorporating a free edge has not been examined with the view of understanding microbuckling.

In developing the analysis, a simple example is considered first in which a single fiber perfectly bonded to a half-plane is subjected to compression. This is done for two reasons: first, to understand the effects of boundary conditions that are applied at the interface of the different materials, particularly from a buckling standpoint, and secondly, to assist in developing the more elaborate analysis that follows, where a more realistic configuration for the composite is chosen in which the entire half-plane is a unidirectionally laminated medium.

2 Problem Formulation

2.1 An Example Problem. Consider the idealized, single fiber composite of unit thickness in the $\hat{z}$-direction, shown in Fig. 2(*a*). For carity of presentation, upper case letters have been used in the figures for coordinate axes corresponding to their lower case counterparts in the text. The composite is sub-

jected to a uniform compression (P/h) per unit thickness normal to the $\hat{x}$, $\hat{y}$-plane of the figure. The relatively "soft" supporting medium (matrix) acts as an *elastic* foundation offering lateral support to the fiber. For convenience, a composite of infinite extent in the $\hat{x}$-direction occupying the space $0 \le y \le \infty$ is considered. Standard notation, such as "E" for Young's modulus and ν for Poisson's ratio is used with the subscripts "f" and "m" to denote properties of the fiber and matrix, respectively. The analysis is carried out for composites typical of those in the aerospace industry where $E_f \gg E_m$. Consequently, the prebuckling deformation of the composite is one of uniform contraction with the compressive load borne essentially by the fiber. Bernoulli-Navier beam theory is used to describe the fiber, while the matrix is modeled as a linearly elastic, homogeneous, and isotropic medium. The prebuckled state for the fiber (a positive sign associated with compression) is described by

$$\epsilon_0 = \frac{P}{E_f h}, \quad v = 0. \tag{5}$$

Next, the governing equations for the fiber in the buckled state are developed. With reference to Fig. 2(b), consider an element of the fiber infinitesimally removed from the straight configuration. It is cut by planes that were parallel to the $\hat{y}$, $\hat{z}$ plane at $\hat{x}$ and $\hat{x}+d\hat{x}$ in the undeformed state. These sections remain plane and normal to the deformed middle surface. With the assumption that rotations are small compared to unity, force equilibrium, and moment equilibrium in the $\hat{x}$, $\hat{y}$ plane results in

$$\frac{dQ}{d\hat{x}} + \sigma - P\frac{d^2v}{d\hat{x}^2} = 0 \tag{6a}$$

$$\frac{dp'}{d\hat{x}} + q = 0 \tag{6b}$$

$$-\frac{d^2M}{d\hat{x}^2} - \frac{h}{2}\frac{dq}{d\hat{x}} + \frac{dQ}{d\hat{x}} = 0. \tag{6c}$$

Here, p' (per unit length in the $\hat{z}$-direction) is the change in the axial force P at buckling, M is the bending moment in the fiber, and v the deflection of the fiber in the $\hat{y}$-direction. σ and q are the interface tractions develped at buckling because the fiber and matrix are bonded at their common interface. In writing equation (6a), the product $p'd^2v/d\hat{x}^2$, which is of second order, has been omitted. The buckling under investigation is infinitesimal. Equation (6b) can be further simplified by noting that

$$p' = hE_f\frac{du_0}{d\hat{x}}, \tag{7}$$

where u_0 is the axial displacement of the fiber due to buckling. Also,

$$M = -EI\frac{d^2v}{d\hat{x}^2}. \tag{8}$$

Combining (6) through (8), the following is deduced

$$E_f I\frac{d^4v}{d\hat{x}^4} + P\frac{d^2v}{d\hat{x}^2} - \frac{h}{2}\frac{dq}{d\hat{x}} - \sigma = 0$$

$$q + hE_f\frac{d^2u_0}{d\hat{x}^2} = 0. \tag{9}$$

Continuity of displacements at the common interface requires

$$u_0 - \frac{h}{2}\frac{dv}{d\hat{x}}\bigg|_{\hat{y}=\frac{h}{2}} = u_m|_{y=0}$$

$$v\Big|_{\hat{y}=\frac{h}{2}} = v_m|_{y=0}. \tag{10}$$

Periodic perturbations in $u(\hat{x})$ and $v(\hat{x})$ of sinusoidal form about the trivial solution (5), with an arbitrary wavelength, λ, are investigated. Then, one seeks the critical value of P required to maintain this disturbance; q and σ are obtained in terms of the fiber displacements v and u_0. This requires the solution of the elastic displacement equations of equilibrium in the matrix.

2.2 The Matrix Problem. With reference to Fig. 2(c), it is necessary to solve

$$2\frac{\partial^2 u_m}{\partial x^2} + (1-\nu_m)\frac{\partial^2 u_m}{\partial y^2} + (1+\nu_m)\frac{\partial^2 v_m}{\partial x \partial y} = 0$$

$$2\frac{\partial^2 v_m}{\partial y^2} + (1-\nu_m)\frac{\partial^2 v_m}{\partial x^2} + (1+\nu_m)\frac{\partial^2 u_m}{\partial x \partial y} = 0, \tag{11}$$

which are the elastic displacement equations of equilibrium with the approximation of *plane stress* in the x, y-plane, subject to the following boundary conditions:

$$\text{at } y = 0, \quad u_m = U\cos\alpha x, \quad v_m = V\sin\alpha x \tag{12a}$$

$$\text{as } y \to \infty, \quad u_m \to 0, \quad v_m \to 0. \tag{12b}$$

Here, $\alpha = 2\pi/\lambda$ and U, V are arbitrary constants. In writing (12), the form of the buckled displacements of the fiber is assumed as

$$u_{0f} = B\cos\alpha\hat{x}, \quad v_f = A\sin\alpha\hat{x}. \tag{13}$$

The solution of (11) proceeds in the following manner. Let

$$u_m = \psi(y)\cos\alpha x, \quad v_m = \phi(y)\sin\alpha x. \tag{14}$$

Using (14) in (11), and elimination of ϕ(or ψ), results in the following ordinary differential equation for $\psi(\phi)$

$$\psi^{IV} - 2\alpha^2\psi^{II} + \alpha^4\psi = 0, \tag{15}$$

where $(\,)^I \equiv d/dy$; a similar equation results for ϕ.

The solution of (15), subject to the second condition in (12), is

$$\psi = (C_3 y + C_4)e^{-\alpha y}$$

and similarly, (16)

$$\phi = (D_3 y + D_4)e^{-\alpha y}.$$

Here the Cs and Ds are related by

$$C_4 = \frac{D_3}{\alpha}\left[\frac{(3-\nu_m)}{(1+\nu m)}\right] - D_4, \quad C_3 = -D_3. \tag{17}$$

Equation (17) is obtained by substituting (16) into (11). Incorporating the first of (12), one arrives at

$$u_m(x,0) = \left[\frac{D_3}{\alpha}\frac{(3-\nu_m)}{(1+\nu_m)} - D_4\right]\cos\alpha x, \quad v_m(x,0) = D_4\sin\alpha x \tag{18}$$

with

$$D_4 = V, \quad D_3 = \alpha\frac{(1+\nu_m)}{(3-\nu_m)}U + \alpha\frac{(1+\nu_m)}{(3+\nu_m)}V. \tag{19}$$

Next, the surface tractions q and σ are computed;

$$\tau_{xy} = G_m\left[\frac{\partial u_m}{\partial y} + \frac{\partial v_m}{\partial x}\right] = G_m[\psi' + \alpha\phi]\cos\alpha x.$$

Thus,

$$\tau_{xy}(x, 0) \equiv q(x, 0) = G_m\left[2\alpha \frac{(1-\nu_m)}{(3-\alpha)} V - \frac{4\alpha}{(3-\nu_m)} U\right]\cos\alpha x. \tag{20}$$

The normal stress

$$\sigma_y = \frac{E_m}{(1-\nu_m^2)}\left[\frac{\partial v_m}{\partial y} + \nu_m \frac{\partial u_m}{\partial x}\right]$$

$$= \frac{E_m}{(1-\nu_m^2)}\left[\phi' - \nu_m \alpha \psi\right]\sin\alpha x.$$

Thus,

$$\sigma_y(x, 0) \equiv \sigma(x, 0) = -\frac{E_m \alpha}{(1+\nu_m)(3-\nu_m)}\left[2V - U(1-\nu_m)\right]\sin\alpha x. \tag{21}$$

Using (13) and (12a), the following is obtained:

$$V = A$$
$$U = B - \frac{h\alpha}{2} A. \tag{22}$$

Substituting (20) through (22) into (9), the following system of equations results

$$(a_1 - \epsilon_0)A + b_1 B = 0$$
$$a_2 A + b_2 B = 0 \tag{23}$$

where

$$a_1 = \frac{\rho^2}{12} + \frac{2\mu}{\rho(1+\nu_m)(3-\nu_m)} + \frac{\mu(1-\nu_m)}{2(3-\nu_m)(1+\nu_m)} + \frac{\mu(\rho+(1-\nu_m))}{2(1+\nu_m)(3-\nu_m)}$$

$$a_2 = \frac{\mu((1-\mu_m)+\rho)}{\rho(1+\nu_m)(3-\nu_m)}$$

$$b_1 = \frac{-\mu}{(1+\nu_m)(3-\nu_m)} - \frac{\mu(1-\nu_m)}{\rho(3-\nu_m)(1+\nu_m)}$$

$$b_2 = \frac{2\mu}{\rho(1+\nu_m)(3-\nu_m)} + 1,$$

and the following nondimensionalizations have been used

$$\rho = h\alpha = \frac{2\pi h}{\lambda}$$
$$\mu = \frac{E_m}{E_f} \tag{24}$$

For nontrivial solutions for A and B, one requires

$$\begin{vmatrix} (a_1 - \epsilon_0) & b_1 \\ a_2 & b_2 \end{vmatrix} = 0. \tag{25}$$

The condition (25) implies that

$$\epsilon_0 = a_1 + a_2\left(\frac{b_1}{b_2}\right). \tag{26}$$

2.3 Results and Discussion. To illustrate the results, the material properties listed in Table 1 have been chosen. These correspond to the two fiber/matrix systems, designated as T300/BP907 and IM7/8551-7. From now on, these shall be referred to as BP907 and IM7, respectively.

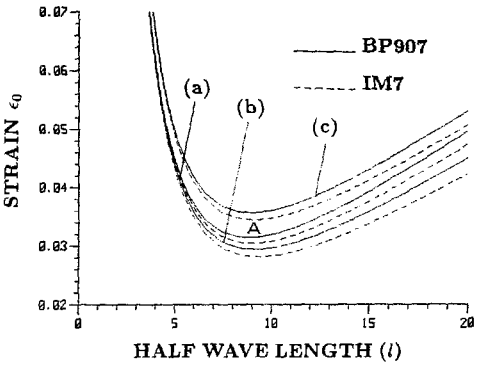

Fig. 3 Variation of ϵ_0 with nondimensional half wavelength l. Comparison of predictive models; curve (a) is Gough (1939), curve (b) is Reissner (1937), and curve (c) is the present; dashed line—IM7, solid line—BP907

Table 1

	BP907	IM7
$\frac{E_f}{E_m}$	74.2	79.3
ν_m	0.38	0.33

Figure 3 shows the variation of ϵ_0, with the nondimensional half wavelength $l(l=\lambda/2h)$. In this plot, the present results (solid curve for BP907 and dashed curve for IM7) are compared with those of two other models. The first one, Gough et al. (1939), is obtained by neglecting the presence of the interface shear traction q. In that calculation, instead of the continuity conditions, equations (10) are replaced by the requirement that the surface of the matrix ($y=0$) is constrained to satisfy

$$\epsilon_x = 0$$
$$v = v_m. \tag{27a}$$

In the second model (Reissner (1937)) the surface of the matrix is taken to be free from shearing stress. This amounts to satisfying (at $y=0$)

$$v = v_m$$
$$\tau_{xy} = 0. \tag{27b}$$

In computing the critical strain, the models of Gough (1939) and Reissner (1937) do not account for the interface shear traction developed at buckling. From Fig. 3 the minimum values of ϵ_0, such as those corresponding to point A, are identified as the buckling strain.

The manner in which the buckling strain in affected as a function of the ratio of Young's moduli of the constituents E_f/E_m is shown in Fig. 4(a). The corresponding critical wavelength variation is depicted in Fig. 4. Notice that a large disparity in Young's moduli between fiber and matrix ($E_f \gg E_m$) leads to a gradually decreasing value of critical strain, with the rate of this decrease diminishing as the limit $E_f/E_m \to \infty$ is approached. Further, as expected, the agreement between the present calculation and those of Gough et al. (1939) and Reissner (1937) improves as this limit is approached. Also, as $E_f/E_m \to \infty$, by holding E_f constant and letting $E_m \to 0$, which corresponds to a gradual disappearence of the matrix, the Euler formula, $\epsilon_{cr} = \rho^2/12$, is obtained from the present result (26). Next, consider the case of $E_f/E_m \to 1$. Here, there is a noticeable difference in the predicted values of ϵ_0 between the three calculations. However, in the range $E_f/E_m \leq 20$, the predicted critical nondimensional half wavelength l is less than 5. Thus, in this situation where the critical wavelength becomes comparable to the thickness of the fiber, use of a one-dimensional theory, such as technical beam theory in describing the fiber, is inappropriate. The effect of Poisson's ratio on the buckling strain and critical half

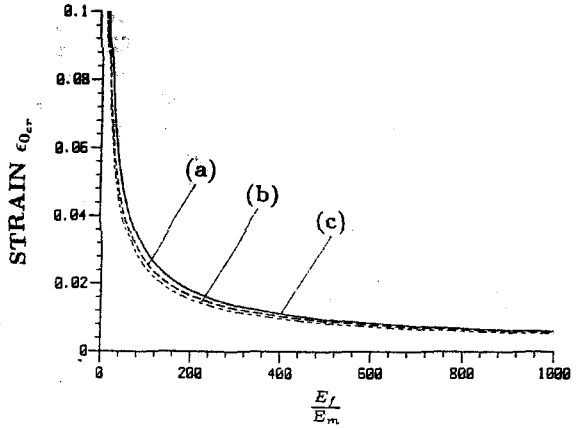

Fig. 4(a) Variation of critical ϵ_0 with ratio of Young's moduli E_f/E_m; curves (a), (b), and (c) as in Fig. 3

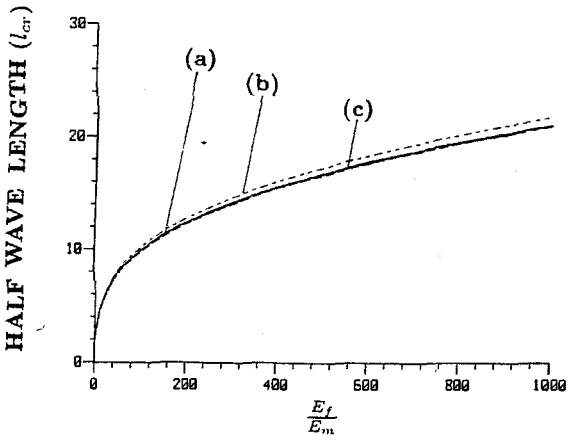

Fig. 4(b) Variation of critical half wavelength (l_{cr}) with ratio of Young's moduli E_f/E_m; curves (a), (b), and (c) as in Fig. 3

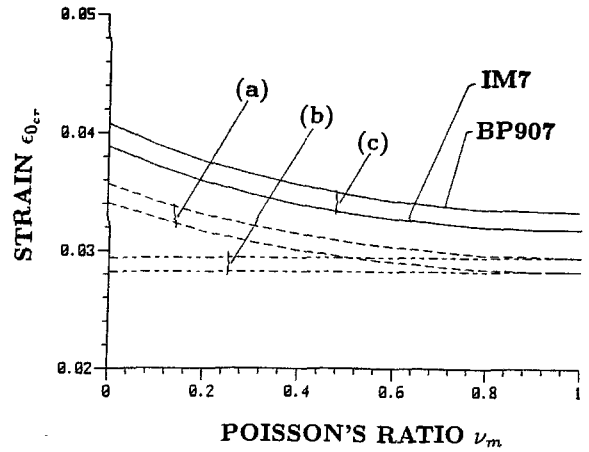

Fig. 5(a) Effect of Poisson's ratio on critical strain ϵ_0; curves (a), (b), and (c) as in Fig. 3

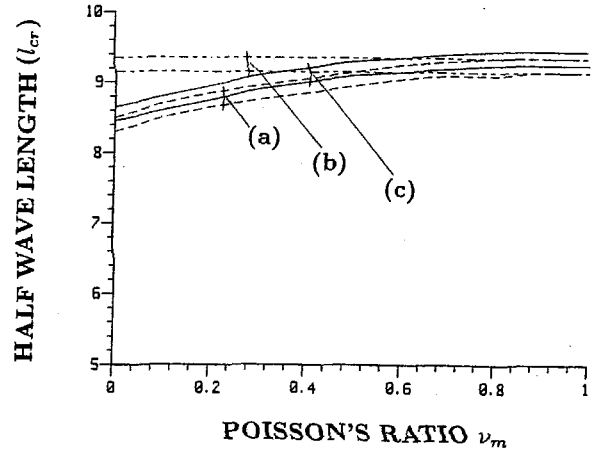

Fig. 5(b) Effect of Poisson's ratio on critical half wavelength l_{cr}; curves (a), (b), and (c) as seen in Fig. 3

wavelength can be inferred from Fig. 5. Here, it is seen that when $\nu_m = 0$ (a condition which constrains the matrix to behave such that $\epsilon_y = \epsilon_z = 0$ at buckling), the buckling strain is higher than for cases $\nu_m \geq 0$. This is to be expected because the constraining condition "stiffens" the matrix at buckling.

In summary, it is observed that the effect of the interface shear traction occurring at buckling is to introduce small periodic fluctuations in the axial thrust acting on the fiber (denoted by p' in the formulation). Further, this shear traction also introduces bending moments because of its eccentricity with respect to the centerline of the fiber. These effects have been included in the present formulation.

The stresses in the matrix associated with the sinusoidally-buckled form of the fiber contain the multiplier $e^{-\alpha y}$, and thus diminish as y increases. At a sufficiently large value of y, they may be regarded as negligible. Thus, the coefficient $'\alpha_{cr}'$ in the exponent characterizes a boundary layer depth into the matrix to which any surface disturbance can be felt. The quantity "αy" can be rewritten as,

$$\alpha y = \frac{2\pi}{\lambda} y = \frac{\pi}{l} \cdot \left(\frac{y}{h}\right). \tag{28}$$

Figure 4(b) shows a plot of l_{cr} against the ratio E_f/E_m. It is seen that for a "soft" matrix ($E_f/E_m = 500$, say), the surface disturbance is felt to a larger depth than for a "hard" matrix ($E_f/E_m = 50$, say). This result can be interpreted in the light of more realistic composites. Suppose a unidirectional laminated composite contains several fibers. Then, so long as the fiber spacing is larger than a certain minimum value, the interaction between adjacent fibers will be negligible, and the one-fiber model presented here can be used as a measure of the compressive strength of the composite. However, in order to maximize the specific stiffness of the composite (the E/ρ ratio), one needs to attain a high volume fraction of fibers. This makes the spacing between fibers (expressed more readily in terms of fiber volume fraction $V_f = (h/h+2c)$ small compared with h. Typical values of V_f range from $0.5-0.6$ for fiber-reinforced laminated systems that are currently in use. Thus, it is informative to address the more general problem of a laminated medium containing many fibers under compressive loading (Fig. 6(a)). There are several ways to approach this problem. In the spirit of the previous analysis, this can be modeled as a problem of a single fiber resting on an equivalent orthotropic medium (the "smeared" foundation). However, unlike before, the prebuckling stress state in the "foundation" is quite different. No longer can it be assumed that the totality of the load is borne by the surface fiber alone. Indeed, one is compelled to consider a problem in which the "foundation's" initial stressed state on the buckling of the surface fiber has to be accounted for. Such a consideration can pose difficulties in solving for the displacements of the foundation in the presence of the initial stress, since now a two-dimensional stability problem for the foundation itself has to be considered.

Another approach to the problem is to consider individual fibers separately, and account for the interaction effects between adjacent fibers by analyzing the deformation of the sandwiched elastic matrix at buckling. It is this approach that is followed in the next investigation.

3 Buckling of a Layered Medium

3.1 Problem Formulation. The configuration being studied is shown in Fig. 6(a). Here, the end compression is in-

dicated as being carried entirely by the fibers. To verify this assumption, let P (per unit length in the $\hat{z}$-direction) be the applied load to a "unit cell" of depth $(h+2c)$ in the prebuckled state. Then, the axial compressive stresses in the fiber and matrix are

$$\sigma_{x_f} = \frac{P}{h\left(1+\frac{2c}{h}\frac{E_m}{E_f}\right)}$$

$$\sigma_{x_m} = \frac{P}{h\left(\frac{E_f}{E_m}+\frac{2c}{h}\right)}$$

with

$$\frac{2c}{h} = \left(\frac{1-V_f}{V_f}\right).$$

These reduce to $\sigma_{x_f} = P/h$ and $\sigma_{x_f} \gg \sigma_{x_m}$, so long as $(E_f/E_m) \gg ((1-V_f)V_f)$ and $E_f \gg E_m$, which is the case in the present investigation. Thus, the prebuckled state of the composite is as described by (5), with the end compression load carried entirely by the fibers. The matrix acts as an elastic foundation. Next, consider the composite in the buckled configuration (Fig. 6(b) and 6(c)). Then, considering the equilibrium of a typical fiber, the following set of equations result for the surface fiber ($N=1$) and the nth fiber ($N=n$), respectively. (Here an extra subscript n designates quantities associated with the nth fiber.)

Surface Fiber.

$$E_f I \frac{d^4 v_1}{d\hat{x}^4} + P\frac{d^2 v_1}{d\hat{x}^2} - \sigma_{u_1} - \frac{h}{2}\frac{dq_{u_1}}{d\hat{x}} = 0$$

$$q_{u_1} + hE_f \frac{d^2 u_{0_1}}{d\hat{x}^2} = 0. \tag{29}$$

nth Fiber.

$$E_f I \frac{d^4 v_n}{d\hat{x}^4} + P\frac{d^2 v_n}{d\hat{x}^2} - [\sigma_{u_1} - \sigma_{L_{n-1}}] - \frac{h}{2}\frac{d}{d\hat{x}}[q_{u_n} + q_{L_{n-1}}] = 0$$

$$[q_{u_n} - q_{L_{n-1}}] + hE_f \frac{d^2 u_{0_n}}{d\hat{x}^2} = 0. \tag{30}$$

In order to proceed with the solution of (29) and (30), the shearing and normal tractions (q, σ) developed at the fiber/matrix interface at buckling have to be determined. This can be done by considering the deformation of a typical matrix layer sandwiched between any two fibers. Thus, isolate the nth and $(n+1)$st fibers and the matrix in between (Fig. 6(c)). To proceed, solving for the displacements in the matrix layer, some boundary conditions have to be imposed at the fiber/matrix interface. As before, sinusoidal perturbations in $u(\hat{x})$, $v(\hat{x})$ are investigated about the trivial solution (5). Thus, for the nth fiber it is assumed,

$$u_{0n} = U_{0n}\cos\alpha\hat{x}$$
$$v_n = V_n \sin\alpha\hat{x}. \tag{31}$$

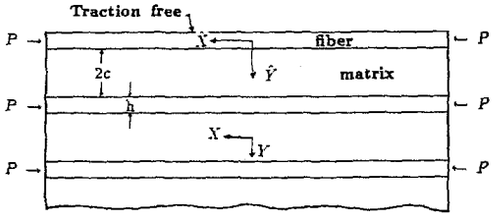

Fig. 6(a) Configuration for unidirectional laminated composite

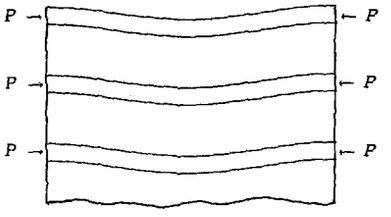

Fig. 6(b) Buckled configuration of laminated composite

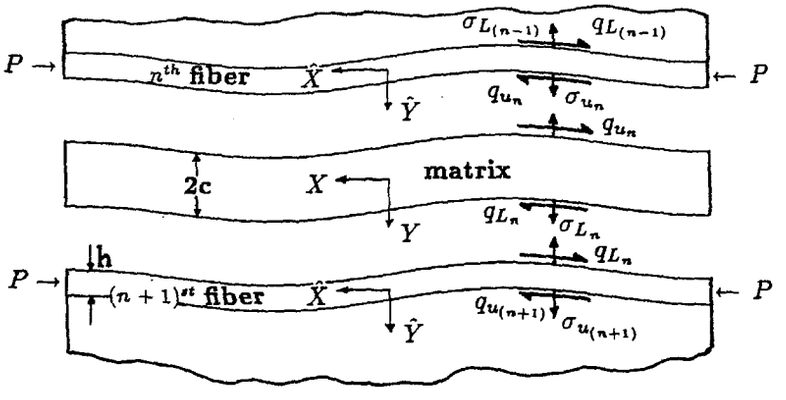

Fig. 6(c) Isolated portion of buckled configuration; nth, $(n+1)$st fibers and sandwiched matrix

U_{0n}, V_n are the unknown amplitudes of the perturbations $u_n(\hat{x})$, $v_n(\hat{x})$, respectively, of the nth fiber.

Next, the deformation of the matrix strip between the nth and $(n+1)$st fibers is considered. With reference to Fig. 6(*c*), it is required to solve (11) in the matrix subject to the following boundary conditions

nth fiber/matrix interface

$$u_{0n} - \frac{h}{2}\frac{dv_n}{d\hat{x}}\bigg|_{\hat{y}_n=\frac{h}{2}} = u_m|_{y=-c}$$
$$v_n\big|_{\hat{y}_n=\frac{h}{2}} = v_m|_{y=-c} \tag{32a}$$

$(n+1)$st fiber/matrix interface,

$$u_{0(n+1)} + \frac{h}{2}\frac{dv_{(n+1)}}{d\hat{x}}\bigg|_{\hat{y}_{n+1}=-\frac{h}{2}} = u_m|_{y=c}$$
$$v_{(n+1)}\big|_{\hat{y}_{n+1}=-\frac{h}{2}} = v_m|_{y=c}. \tag{32b}$$

Notice that by confining attention to the nth and $(n+1)$st fibers and the sandwiched matrix in between, it is possible to generate the governing equations for *any fiber*. The interface continuity conditions for displacements are completely specified by (32) in that, at *every* fiber/matrix interface, one of the conditions (32) will apply.

The solution of (11) subject to (32) is,

$$\begin{aligned} u_m(x,y) &= (C_1\cosh\alpha y + C_2\sinh\alpha y + C_3 y\cosh\alpha y \\ &\quad + C_4 y\sinh\alpha y)\cos\alpha x \\ v_m(x,\hat{y}) &= (D_1\cosh\alpha y + D_2\sinh\alpha y + D_3 y\cosh\alpha y \\ &\quad + D_4 y\sinh\alpha y)\sin\alpha x, \end{aligned} \tag{33}$$

with

$$\begin{aligned} D_1 &= C_2 - \frac{C_3}{\alpha}\left(\frac{3-\nu_m}{1+\nu_m}\right) \\ D_2 &= C_1 - \frac{C_4}{\alpha}\left(\frac{3-\nu_m}{1+\nu_m}\right) \\ D_3 &= C_4 \\ D_4 &= C_3. \end{aligned} \tag{34}$$

Here, $C_i\,(i=1,4)$ is related to the unknown amplitudes of the adjacent fibers U_{0n}, $U_{0(n+1)}$, V_n, $V_{(n+1)}$ through the conditions (32) by

$$\begin{aligned} C_1 &= m_{11}\left[U_{0(n+1)} + U_{0n} + \frac{\rho}{2}(V_{(n+1)} - V_n)\right] \\ &\quad + m_{12}[V_{(n+1)} - V_n] \\ C_2 &= m_{21}\left[U_{0(n+1)} - U_{0n} + \frac{\rho}{2}(V_{(n+1)} + V_n)\right] \\ &\quad + m_{22}[V_{(n+1)} + V_n] \\ \frac{C_3}{\alpha} &= m_{31}\left[U_{0(n+1)} - U_{0n} + \frac{\rho}{2}(V_{(n+1)} + V_n)\right] \\ &\quad + m_{32}[V_{(n+1)} + V_n] \\ \frac{C_4}{\alpha} &= m_{41}[U_{0(n+1)} + U_{0n} + \frac{\rho}{2}(V_{(n+1)} - V_n)\big] \\ &\quad + m_{42}[V_{(n+1)} - V_n]. \end{aligned} \tag{35}$$

The constants $m_{11}, \ldots m_{14}$ and $m_{21}, \ldots m_{24}$ are given in Appendix A.

Having obtained the displacement field for the matrix strip (32) in terms of the boundary values $U_{0(n+1)}$, U_n, $V_{(n+1)}$, V_n, the surface tractions σ_{u_n}, $\sigma_{L_{(n-1)}}$, q_{u_n}, $q_{L_{(n-1)}}$ acting on the nth fiber can be computed.

Thus,

$$\begin{aligned} \sigma_{u_n} &= \frac{E_m\alpha}{(1-\nu_m^2)}[U^1{}_nP_{u_1} + U_{(n+1)}P_{u_2} + V_nP_{u_3} \\ &\quad + V_{(n+1)}P_{u_4}]\sin\alpha x \\ \sigma_{L_{(n-1)}} &= \frac{E_m\alpha}{(1-\nu_m^2)}[U_{(n-1)}P_{L_1} + U^2{}_nP_{L_2} + V_{(n-1)}P_{L_3} \\ &\quad + V_nP_{L_4}]\sin\alpha x \\ q_{u_n} &= G_m\alpha[U^1{}_nR_{u_1} + U_{(n+1)}R_{u_2} + V_nR_{u_3} \\ &\quad + V_{(n+1)}R_{u_4}]\cos\alpha x \\ q_{L_{(n-1)}} &= G_m\alpha[U_{(n-1)}R_{L_1} + U^2{}_nR_{L_2} + V_{(n-1)}R_{L_3} \\ &\quad + V_nR_{L_4}]\cos\alpha x, \end{aligned} \tag{36}$$

where

$$\begin{aligned} U^1{}_n &= U_{0n} - \frac{\rho}{2}V_n \\ U^2{}_n &= U_{0n} + \frac{\rho}{2}V_n \\ U_{(n+1)} &= U_{0(n+1)} + \frac{\rho}{2}V_{n+1} \\ U_{(n-1)} &= U_{0(n-1)} - \frac{\rho}{2}V_{n-1}. \end{aligned} \tag{37}$$

Expressions for $P_{u_1}, \ldots, R_{u_1} \ldots$, etc. are given in Appendix A. Substituting (36) into (30), the following system of equations for the nth fiber are obtained:

$$\begin{aligned} &\frac{\rho^2}{12}V_n - \epsilon_0 V_n - \frac{\mu}{\rho(1-\nu_m^2)}F_1(U_{0(n-1)}, U_{0n}, U_{0(n+1)}, \\ &\quad V_{n-1} \ldots V_n) + \frac{\mu^*}{2}F_2(U_{0(n-1)}, \ldots) = 0 \\ &\frac{\mu^*}{\rho}F_3(U_{0(n-1)}, \ldots\ldots) - U_{0n} = 0. \end{aligned} \tag{38}$$

Here, $\mu^* = G_m/E_f$. The functions $F_1, \ldots F_3$ are *linear* combinations of the six unknown amplitudes $U_{0(n-1)}$, U_{0n}, $U_{0(n+1)}$, V_{n-1}, V_n, V_{n+1}. These functions are given in Appendix A. Similarly, for the surface fiber from (29), the following equations are obtained

$$\begin{aligned} &\frac{\rho^2}{12}V_1 - \epsilon_0 V_1 - \frac{\mu}{\rho(1-\nu_m^2)}F_4(U_{01}, U_{02}, V_1, V_2) \\ &\quad + \frac{\mu^*}{2}F_5(U_{01}, \ldots, V_2) = 0 \\ &\frac{\mu^*}{\rho}F_6(U_{01}, \ldots\ldots V_2) - U_{01} = 0. \end{aligned} \tag{39}$$

The functions $F_4, \ldots F_6$ are also given in Appendix A.

The system of equations (38) and (39) can be conveniently arranged in the following form

$$[\hat{Q}^*][\mathbf{u}_1] + [\hat{Q}][\mathbf{u}_2] = 0 \tag{40a}$$
$$[Q][\mathbf{u}_{n-1}] + [\hat{Q}][\mathbf{u}_n] + [\bar{Q}][\mathbf{u}_{n+1}] = 0, \tag{40b}$$

where elements of the (2×2) matrices Q, $\hat{Q}$, etc., are arranged in Appendix B and

$$\mathbf{u}_n = \begin{bmatrix} u_{0n} \\ v_n \end{bmatrix}.$$

It is of interest to seek solutions to the perturbation amplitudes (U_{0n}, V_n) that exhibit a decay into the interior of the half-plane under consideration. Thus, one seeks values of

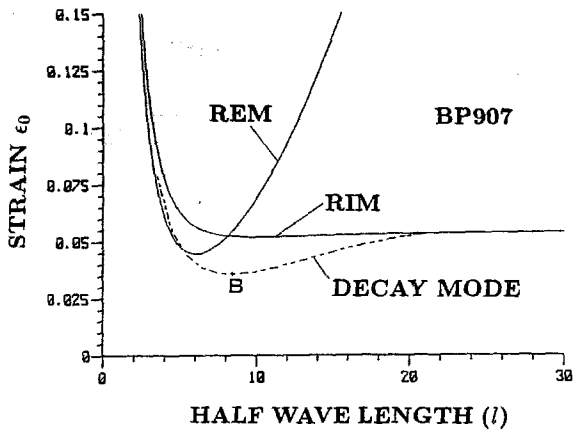

Fig. 7(a) Variation of ϵ_0 with nondimensional half wavelength l for T300/BP907. "decay mode" denotes present results. $V_f = 0.1$

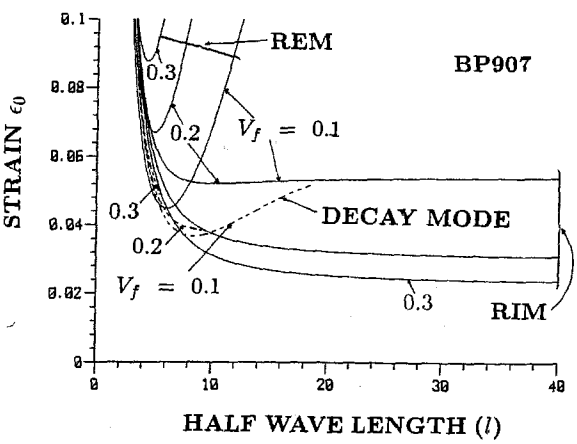

Fig. 7(b) Variation of ϵ_0 with nondimensional half wavelength l for T300/BP907. "decay mode" denotes present results; V_f as a parameter

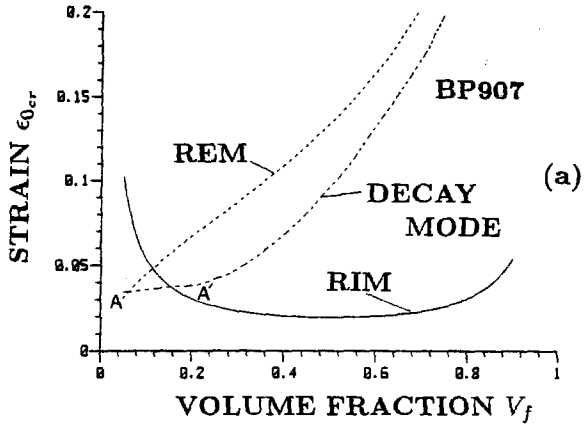

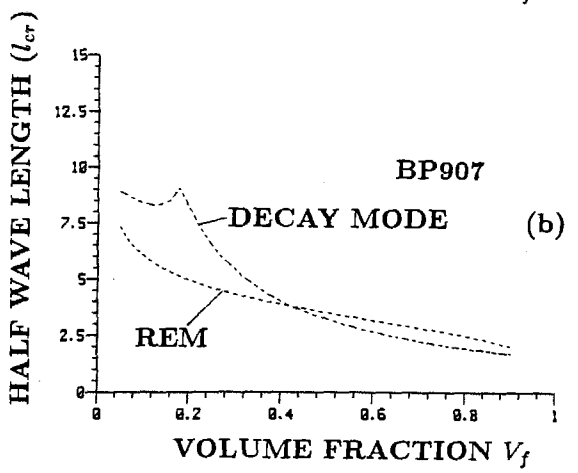

Fig. 8(a) Variation of critical ϵ_0 with fiber volume fraction V_f for T300/BP907 and (b) variation of critical half wavelength l_{cr} with fiber volume fraction V_f for T300/BP907

ϵ_0 that permit this behavior. Of all possible ϵ_0 that fall into this category, the minimum ϵ_0 is identified as the buckling "load" of the system. Thus, the following problem is considered.

We are required to solve (40) subject to the condition

$$U_{01},\ V_1 \quad \text{finite}$$
$$U_{0n},\ V_n \to 0 \text{ as } n \to \infty. \tag{41}$$

Notice that (40) subject to (41) is a *difference equation eigenvalue problem*. Here, ϵ_0 is the eigenvalue sought and the amplitudes U_{0n}, V_n are the associated eigenfunctions. The boundary conditions (41) are physically motivated to conform to the experimental observations discussed in (Hahn and Williams, 1986; Sohi, Hahn, and Williams, 1984; Waas and Babcock, 1989). The solution proceeds in the following manner: First, (40*b*) is solved using the boundary condition for large n. This enables one to find the general solution for U_{0n}, V_n up to two arbitrary constants. Then, using the first of conditions (41) and the obtained general solution, substitute for U_{01}, V_1 into (40*a*). This results in a (2×2) system of homogeneous equations for the two as yet undetermined constants. Vanishing of the determinant associated with this system gives the required condition to obtain ϵ_0. Unlike in the previous case, it is not possible to obtain an explicit expression for ϵ_0 (see (26)). This is because each member of the matrix associated with the final system of equations is a function of ϵ_0. Thus, we obtain an equation implicit in ϵ_0 of the form

$$G(\epsilon_0, l) = 0. \tag{42}$$

Newton's method is used to solve (42) for a specified l. Details of the solution process can be found in Waas 1987. Depending on the geometry and material properties of the composite, several cases will be discussed next.

3.2 Results and Discussion. Results are computed for composites whose material properties are listed in Table 1. For clarity of presentation, the results are displayed in the (ϵ_0, l) plane. In the discussion to follow, the term "decaying solution" is used to refer to solutions of (40) subject to (41). For comparison purposes we first present solutions to (40) subject to

$$U_{0n} = 0, \ \ldots\ V_{(n-1)} = V_{(n)} = V_{(n+1)} \ \ldots \tag{43}$$

which is the displacement field assumed in RIM (abbreviation for Rosen's in-plane mode (1965)). The value of ϵ_0 predicted by such a specialization is obtained by substituting (43) into (40*b*). One then finds

$$\epsilon_0 = \hat{q}_{12}. \tag{44}$$

Values of (ϵ_0, l) conforming to (44) are indeed the RIM prediction. However, in order that (44) be a solution to (40), it must in addition satisfy the required boundary condition for large n. Clearly, this is not the case. The reason is that the Rosen shear mode result holds only for a composite of infinite extent, without recourse to a traction-free edge. Furthermore, the Rosen result

$$\sigma_{cr}\,|_{\min} = \frac{G_m}{(1 - V_f)}$$

is obtained in the limit $l \to \infty$, implying a mode of buckling with a long wavelength. Thus, the Rosen prediction corresponds to buckling of an *infinite* medium where *all* wavelengths ($l \gg 1$) are admissible solutions. Physically, the RIM prediction furnishes values of ϵ_0 corresponding to the equilibrium of the composite in a nontrivial configuration in which *every fiber buckles in an identical manner*. Where appropriate, the RIM prediction is included in the results presented for comparison purposes.

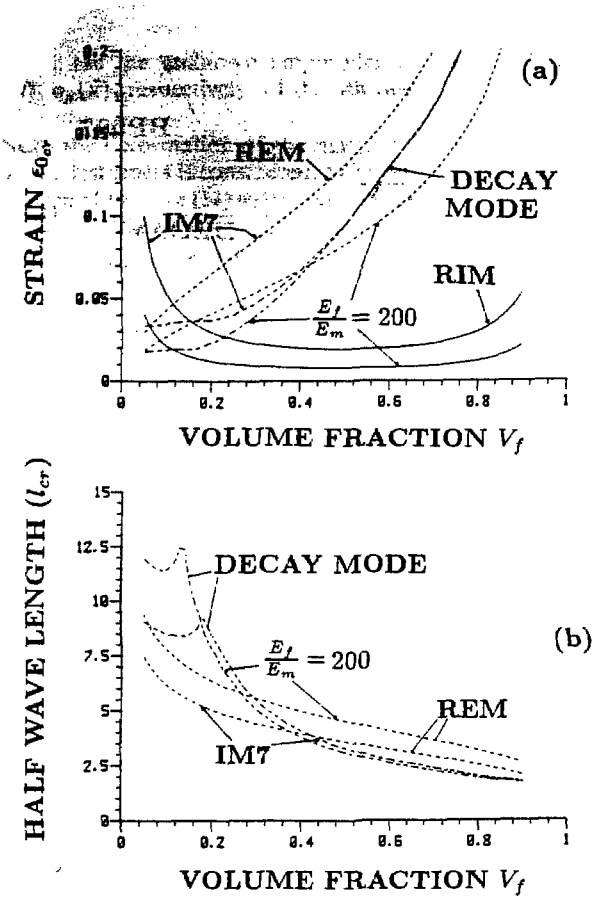

Fig. 9(a) Variation of critical ϵ_0 with fiber volume fraction V_f; comparison of IM7/8551-7 with composite of $E_f/E_m = 200$, and (b) variation of critical half wavelength l_{cr} with fiber volume fraction V_f; comparison of IM7/8551-7 with composite of $E_f/E_m = 200$.

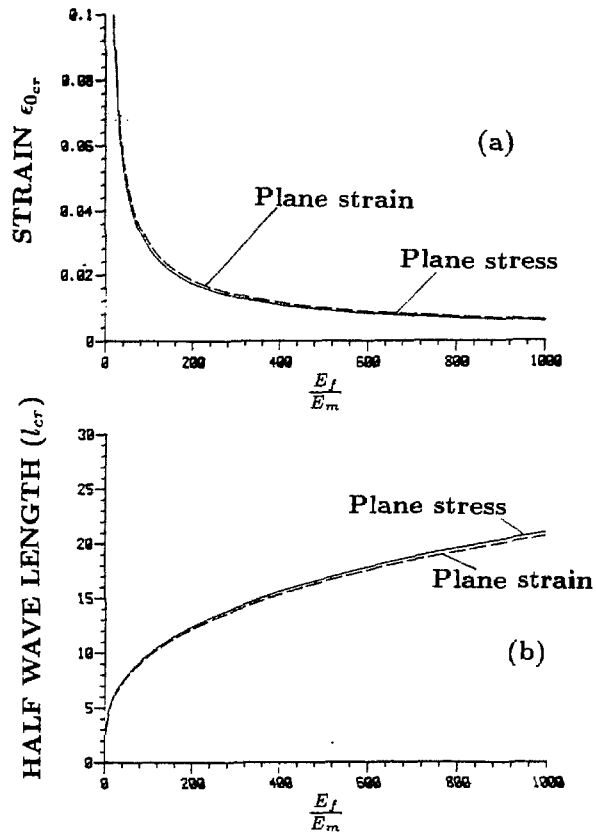

Fig. 10 Comparison of plane-stress and plane-strain approximations for BP907 single fiber composite; (a) $\epsilon_{0_{cr}}$ variation and (b) l_{cr} variation

In Fig. 7(*a*), a plot of variation of strain with l for a composite with a low fiber volume fraction $V_f = 0.1$ is shown. In this figure, the result obtained from the present analysis has been compared with those of RIM and REM (Rosen extensional mode). Notice that the buckling strain as predicted by the present analysis, and marked as point B, is lower than both the RIM and REM predictions. Similar curves for other values of V_f are shown in Fig. 7(*b*). Here, the minimum point of the curves marked as "decay mode" shifts to the right with increasing values of V_f. Beyond a certain value of V_f, the minimum is found to disappear. The nonexistence of a true minimum implies a continuous dependence of ϵ_0 on the half wavelength l. Thus, for a fixed value of E_f/E_m, a critical decay buckling mode of short wavelength exists below a certain V_f. Above this value of V_f, a short wavelength buckling instability is still present but shows a continous dependence on l. With increasing V_f, the buckling strain increases, while the corresponding critical half wavelength decreases as is shown in Figs. 8(*a*) and 8(*b*). However, in this limit ($V_f \to 1$), the critical half wavelength becomes comparable to the thickness of a fiber ($l \approx 1$). In such cases, treating the fiber via beam theory is inadequate. To properly address this question requires modeling a fiber as a two-dimensional continuum. This aspect is not considered in this presentation.

A critical strain (ϵ_{cr}) is defined by points corresponding to such as B in Fig. 7(*a*), and when a true minimum does not exist, the minimum of all admissible (ϵ_0, l). Then, Fig. 9(*a*) shows plots of ϵ_{cr} against the volume fraction V_f. In this figure, curves for a composite of large E_f/E_m (=200) and $\nu_m = 0.3$ have also been included for comparison purposes. The corresponding plots for the corresponding critical wavelength are shown in Fig. 9(*b*). In Fig. 8(*a*), the portion of the curve marked A-A′ is a region of almost constant strain. This region spans a range of V_f that is large for small values of the composite's E_f/E_M. This can be inferred from Fig. 9(*a*). The "section" A-A′ corresponds to the value of ϵ_0 obtained from the previous analysis for a single-fiber composite. Physically, this implies that for values of V_f, less than that corresponding to point A′, the fiber spacing is large enough that there are no interactions between fibers. Thus, the buckling is as predicted for a single-fiber composite. Beyond point A′, one can no longer ignore this interaction effect. That this is so was emphasized in our previous discussion on a single-fiber composite. There, the existence of a certain critical depth into the matrix to which any surface effects were felt was discussed. It was noted that for a "soft" composite ($E_f/E_m \approx 200$, say) this depth was larger than for a "hard" composite ($E_f/E_m \approx 50$, say). Thus, here it is not surprising that the region of constant strain A-A′ persists further for the harder composite (Fig. 9(*a*)). However, it is seen that in situations where the interaction effect is present, the present decay mode prediction yields a higher value of buckling strain as compared with the RIM prediction for a composite of infinite extent. Experimental results reported in the literature show some scatter (Shuart, 1985) in the data on compressive strength. The RIM prediction, when compared with this data, can be in error by as little as 40 percent (June et al. 1969) to as large as by an order of magnitude (Shuart, 1985; Hahn and Williams, 1986; Sohi, Hahn, and Williams, 1984; Lager and June, 1969; Waas and Babcock, 1989; Waas, 1987).

Before discussing possible causes for such a discrepancy, the difference in the results between a *plane-stress* and *plane-strain* approximation for the perturbation problem will be addressed. The plane-strain result can be generated by making appropriate substitutions for the elastic constants. Results are computed for the BP907 composite. For the single fiber case, Fig. 10 shows the critical strain and critical half wavelength

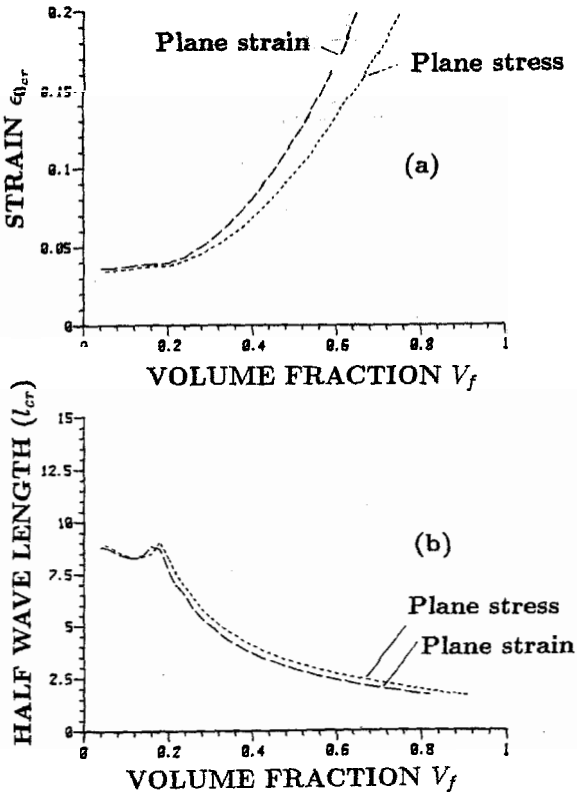

Fig. 11 Comparison of plane-stress and plane-strain approximations for BP907 unidirectional composite; (a) $\epsilon_{0_{cr}}$ variation; (b) l_{cr} variation

variation as a function of (E_f/E_m). With the plane-strain approximation, the computed $\epsilon_{0_{cr}}$ is slightly larger than the corresponding plane-stress result, while l_{cr} is slightly lower. The Poisson's ratio of the fiber is assumed as 0.2. The corresponding results for the unidirectional composite exhibit a similar trend as shown in Fig. 11.

It was seen that values of $\epsilon_{0_{cr}}$ calculated for the RIM result and the present investigation overestimated the experimentally observed buckling strains. In addition, the present decay mode result is higher than the RIM result. The reason for this latter discrepancy is that the decay mode, which accounts for interaction between adjacent fibers, yields a critical wavelength that is a small multiple of the fiber diameter as compared with the longer wavelength RIM result. Further, the decay buckling mode is two-dimensional involving a dependence on both the $\hat{x}$ and $\hat{y}$-directions, while the RIM is essentially one-dimensional, presuming that *all fibers* buckle in an identical manner. Thus, the RIM model is less constrained than the present model. However, it is unrealistic as compared with recent experimental findings reported by Hahn and Williams (1986), Sohi et al. (1984), Hahn et al. (1986), and Waas et al. (1989), which indicate a decay mode type of buckling. For example, in Waas and Babcock (1989), real-time holographic interferometry coupled with optical microscopy are used to capture the origins of compressive failure, which is seen to originate at a traction-free edge. In Hahn and Williams (1986) and Sohi, Hahn, and Williams (1984) evidence of multiple fracture in the damage area was presented. It was also postulated that microbuckling of fibers originated with the buckling of a single fiber, which caused tensile stresses to develop in the matrix in between, thus reducing the buckling load of the adjacent straight fiber. This process progressively involved additional fibers as the damage propagated. Both the RIM and the present model enforce perfect bonding conditions between fibers and matrix. In addition, the fibers are assumed to be perfectly aligned in a regular fashion. Both of these simplifications are unrealistic from a physical viewpoint in that neither are the fibers perfectly aligned nor are they perfectly bonded to the matrix. (Evidence to this effect is presented in Hahn et al. (1986) for example, that show SEM micrographs of the cross-section of typical virgin specimens.) An attempt was made to characterize the imperfect bonding between fibers and matrix in Kulkarni et al. (1973). However, no specific parameter was identified that enables quantifying the imperfect nature of the bonding by a suitable measurement in the laboratory. A recent investigation by Minahen and Knauss (1989), addressing the influence of the bond conditions on the buckling strian, has revealed a fivefold reduction in $\epsilon_{0_{cr}}$ when the displacement constraint at the interface is released. The reasons stated above are the primary causes for the discrepancy between the predictive microbuckling models (RIM and present) and the experimental results reported in the literature (Hahn and Williams, 1986; Sohi, Hahn, and Williams, 1984; Hahn, Sohi, and Moon, 1986; Lager and June, 1969; Waas and Babcock, 1989; Waas, 1987).

5 Conclusions

A simple mechanical model for fiber microbuckling has been considered with a view to understanding the effects of a traction-free edge in initiating the buckling process. For low fiber volume fractions, it is demonstrated that a decay buckling mode furnishes values of critical strain which are below the predictions of the classical Rosen model (1965). At high volume fractions, the predicted critical half wavelength becomes comparable to the fiber thickness, invalidating treating the fibers via technical beam theory. A two-dimensional description of the fibers is employed in another investigation.

These preliminary results have highlighted some drawbacks of existing models for fiber microbuckling and are suggestive of the need for future research in understanding the compressive behavior of fiber composites.

Acknowledgments

This work was supported by NASA Grant No. NSG-1483. The authors are appreciative of this support. The interest and encouragement of Dr. J. H. Starnes, Jr. of NASA-Langley is gratefully acknowledged.

References

Biezeno, C. B., and Hencky, H., 1928, "On the general theory of elastic stability," *Koninklijke akademie van wetenschappen te Amsterdam, Proc.*, Vol. 31.

Biot, M., 1939, "A non-linear theory of elasticity and the linearized case for a body under initial stress," *Phil. Mag.*, Vol. 27, p. 468.

Budiansky, B., 1983, "Micromechanics," *Computers and Structures*, Vol. 16, pp. 3-12.

Chaplin, C. R., 1977, "Compressive fracture in unidirectional glass reinforced plastics," *Journal of Materials Science*, Vol. 12, pp. 347-352.

Dale, W. C., and Baer, E., 1974, "Fiber buckling in composite systems: A model for the ultra-structure of uncalcified collagen tissues," *Journal of Materials Science*, Vol. 9, pp. 369-382.

Dow, N. J., and Gruntfest, I. J., 1960, "Determination of most-needed, potentially possible improvements in materials for ballistic and space vehicles," General Electric Company, Air Force Contract AF 04(647)-269, June.

Evans, A. G., and Adler, W. F., 1983, "Kinking as a mode of structural degradation in carbon fiber composites," *Acta Metallurgica*, Vol. 26, pp. 725-738.

Fried, N., and Kaminetsky, J., 1964, "The influence of material variables on the compressive properties of parallel filament reinforced plastics," *Proceedings of the 19th Annual Technical and Management Conference*, Reinforced Plastics Division, Soc. of the Plastics Industry, Inc., February, pp. (9-A) 1-10.

Goodier, J. N., 1946, "Cylindrical Buckling of Sandwich Plates," ASME JOURNAL OF APPLIED MECHANICS, Vol. 13, pp. A253-A260.

Gough, G. S., et al., 1939, "The stabilization of a thin sheet by a continuous supporting medium," *Journal of the Royal Aero. Society*, August, pp. 12-43.

Hahn, H. T., Sohi, M., and Moon, S., 1986, "Compression failure mechanisms of composite structures," NASA-CR-3988.

Hahn, H. T., and Williams, J. G., 1986, "Compression failure mechanisms in unidirectional composites, March, NASA-TM-85834.